Journal of the Mechanical Behavior of Biomedical Materials 77 (2018) 455–460

Contents lists available at ScienceDirect

Journal of the Mechanical Behavior of Biomedical Materials

journal homepage: www.elsevier.com/locate/jmbbm

A continuum model for tension-compression asymmetry in skeletal muscle

Marcos Latorre[a], Melika Mohammadkhah[b], Ciaran K. Simms[b,*], Francisco J. Montáns[a]

[a] Escuela Técnica Superior de Ingeniería Aeronáutica y del Espacio Universidad Politécnica de Madrid Plaza Cardenal Cisneros, 3, 28040 Madrid, Spain
[b] Trinity Centre for Bioengineering, Department of Mechanical and Manufacturing Engineering, Parsons Building, Trinity College Dublin, College Green Dublin, Ireland

ARTICLE INFO

Keywords:
Chicken pectoralis muscle
Tension/compression asymmetry
Poisson's ratio
Hyperelasticity

ABSTRACT

Experiments on passive skeletal muscle on different species show a strong asymmetry in the observed tension-compression mechanical behavior. This asymmetry shows that the tension modulus is two orders of magnitude higher than the compression modulus. Until now, traditional analytical constitutive models have been unable to capture that strong asymmetry in anisotropic solids using the same material parameters. In this work we present a model which is able to accurately capture five experimental tests in chicken pectoralis muscle, including the observed tension-compression asymmetry. However, aspects of the anisotropy of the tissue are not captured by the model.

1. Introduction

Computational modelling of the human body has many important and practical applications, but the constitutive representation of soft tissues presents challenges. Skeletal muscle presents anisotropic and nonlinear elastic behavior as well as significant viscoelasticity and it is largely incompressible, similar to other biological soft tissues. However, in addition a strong tension-compression asymmetry has now been observed both in porcine and in chicken tissue, where the stress in tension is typically two orders of magnitude higher than in compression in all directions of loading (Takaza et al., 2013; Loocke et al., 2006; Mohammadkhah et al., 2016). This asymmetry is not captured by current constitutive modelling approaches using a single set of material parameters (Mohammadkhah et al., 2016). A recent generalisation of Ogden hyperelasticity in terms of Seth-Hill strains permits some tension/compression asymmetry (Moerman et al., 2016), but it is unclear if it can capture the extent that has been experimentally observed (Takaza et al., 2013; Loocke et al., 2006; Mohammadkhah et al., 2016). Cartilage, shape memory alloys and other materials also exhibit a degree of tension/compression asymmetry, and robust numerical approaches for modelling this response are currently in focus (Zhang et al., 2016; Du and Guo, 2014; Du et al., 2016). In this Technical Note, application of (1) the general mechanics theory of transverse isotropy in the infinitesimal strain range and (2) the recently developed What-You-Prescribe-Is-What-You-Get (WYPiWYG) formulation (Sussman and Bathe, 2009; Latorre and Montáns, 2013, 2014; Crespo et al., 2017) for the finite strain domain to the challenge of tension/compression asymmetry in passive skeletal muscle stress stretch responses are presented. The recent experimental data on chicken pectoralis muscle are used to assess the model fitting capabilities (Mohammadkhah et al., 2016). In particular, the paper assesses the extent to which the models can simultaneously capture the tension and compression aspects of the experimental tests. Some results obtained from the WYPiWYG formulation employed in this work are initially surprising. For this reason the behavior of chicken pectoralis muscle is first assessed in the context of the classical small strain theory, but allowing for different moduli in tension and compression. Since the WYPiWYG formulation is compatible with infinitesimal theory, equivalent results are obtained when using either the small strain theory or the large strain WYPiWYG formulation. In Section 3 we present a stored energy function which simultaneously captures the behavior of the anisotropic five experiments in the finite strain regime.

2. Transversely isotropic infinitesimal strain response

2.1. Strain energy function

Consider an incompressible transversely isotropic material with different axial behavior in tension and compression along its preferred material directions. The tension/compression asymmetry holds even for small strains, so different Young's moduli for tension and compression are obtained from uniaxial testing. The isotropic plane is defined by axes 1 and 2 (direction 1 is the muscle cross-fibre direction) and the muscle fibre direction is axis 3. Then, ε_{11}, ε_{22} and ε_{33} are the axial components in preferred directions of the infinitesimal isochoric strain tensor $\boldsymbol{\varepsilon}$ and $\varepsilon_{13}^{\#} = \sqrt{\varepsilon_{13}^2 + \varepsilon_{23}^2}$ is a composite shear deformation invariant

* Corresponding author.
E-mail addresses: m.latorre.ferrus@upm.es (M. Latorre), mmohamma@tcd.ie (M. Mohammadkhah), csimms@tcd.ie (C.K. Simms), fco.montans@upm.es (F.J. Montáns).

http://dx.doi.org/10.1016/j.jmbbm.2017.09.012
Received 3 March 2017; Received in revised form 19 June 2017; Accepted 6 September 2017
Available online 11 September 2017
1751-6161/

including the shear components ε_{13} and ε_{23}. We can exactly characterize this material with a single isochoric strain energy function of the form

$$\mathscr{W}(\varepsilon_{11}, \varepsilon_{22}, \varepsilon_{33}, \varepsilon_{13}^{\#}) = \omega_{11}(\varepsilon_{11}) + \omega_{11}(\varepsilon_{22}) + \omega_{33}(\varepsilon_{33}) + 2\omega_{13}(\varepsilon_{13}^{\#}) \tag{1}$$

with $\omega_{ii}(\varepsilon)$, $i = \{1, 3\}$, including the tension/compression asymmetry effects, i.e. being piecewise bi-quadratic—subscripts c and t refer to compression and tension, respectively

$$\omega_{ii}(\varepsilon) = \begin{cases} \mu_{ii}^{c}\varepsilon^2 & \text{if} \quad \varepsilon < 0 \\ \mu_{ii}^{t}\varepsilon^2 & \text{if} \quad \varepsilon \geq 0 \end{cases} \tag{2}$$

and $\omega_{13}(\varepsilon_{13}^{\#})$ being quadratic—shear behavior within preferred planes is always symmetric

$$\omega_{13}(\varepsilon_{13}^{\#}) = \mu_{13}(\varepsilon_{13}^{\#})^2 = \mu_{13}(\varepsilon_{13}^2 + \varepsilon_{23}^2) \tag{3}$$

The five deviatoric moduli (material constants) μ_{11}^{c}, μ_{11}^{t}, μ_{33}^{c}, μ_{33}^{t} and μ_{13} characterize the generally bi-linear strain-stress response. This additive, fully uncoupled decomposition in terms of the small strain tensor components in preferred material directions is not a hypothesis within the incompressible infinitesimal strain setting, but rather it is a consequence of taking such a limit in which possible higher order couplings vanish.

2.2. Tension/compression uniaxial tests along fibre and cross-fibre directions

We consider both tension and compression uniaxial tests along both cross-fibre and fibre directions, i.e. four uniaxial tests from which we should be able to determine the four material constants μ_{11}^{c}, μ_{11}^{t}, μ_{33}^{c} and μ_{33}^{t}. In these cases $\varepsilon_{11} \equiv \varepsilon_1$, $\varepsilon_{22} \equiv \varepsilon_2$ and $\varepsilon_{33} \equiv \varepsilon_3$ are isochoric principal strains. From the tensile test along the cross-fibre direction 1 we have—i.e. $\varepsilon_1 > 0$

$$\sigma_1 = \omega'_{11}(\varepsilon_1) + p = 2\mu_{11}^{t}\varepsilon_1 + p \tag{4}$$

where σ_1 is the (Cauchy) stress in axis 1 and p is the pressure Lagrange multiplier associated to the incompressibility constraint $\varepsilon_1 + \varepsilon_2 + \varepsilon_3 = 0$ to be determined from the boundary conditions. In the other axes we have

$$0 = \omega'_{11}(\varepsilon_2) + p = 2\mu_{11}^{c}\varepsilon_2 + p = -2\mu_{11}^{c}\nu_{12}^{t}\varepsilon_1 + p \tag{5}$$

$$0 = \omega'_{33}(\varepsilon_3) + p = 2\mu_{33}^{c}\varepsilon_3 + p = -2\mu_{33}^{c}\nu_{13}^{t}\varepsilon_1 + p \tag{6}$$

where, according to experimental evidence (Mohammadkhah et al., 2016), we have assumed positive Poisson ratios in both axes 2 and 3 during the tensile test in axis 1, i.e. transverse contraction given by $\varepsilon_2 = -\nu_{12}^{t}\varepsilon_1 < 0$ and $\varepsilon_3 = -\nu_{13}^{t}\varepsilon_1 < 0$, so we have used the moduli μ_{11}^{c} and μ_{33}^{c} in Eqs. (5) and (6), respectively. The Lagrange multiplier p may be eliminated and the incompressibility condition (which also results in $\nu_{12}^{t} + \nu_{13}^{t} = 1$) be employed to arrive at

$$\begin{cases} \nu_{12}^{t} = \dfrac{\mu_{33}^{c}}{\mu_{11}^{c} + \mu_{33}^{c}}, \quad \nu_{13}^{t} = \dfrac{\mu_{11}^{c}}{\mu_{11}^{c} + \mu_{33}^{c}} \\ Y_1^{t} = 2\left(\mu_{11}^{t} + \dfrac{\mu_{11}^{c}\mu_{33}^{c}}{\mu_{11}^{c} + \mu_{33}^{c}}\right) \end{cases} \tag{7}$$

where Y_1^{t} is the Young modulus during the tensile test in direction 1. Equivalently, for a compression test

$$\begin{cases} \nu_{12}^{c} = \dfrac{\mu_{33}^{t}}{\mu_{11}^{t} + \mu_{33}^{t}}, \quad \nu_{13}^{c} = \dfrac{\mu_{11}^{t}}{\mu_{11}^{t} + \mu_{33}^{t}} \\ Y_1^{c} = 2\left(\mu_{11}^{c} + \dfrac{\mu_{11}^{t}\mu_{33}^{t}}{\mu_{11}^{t} + \mu_{33}^{t}}\right) \end{cases} \tag{8}$$

where ν_{12}^{c}, ν_{13}^{c} and Y_1^{c} are the Poisson ratios and the Young modulus during the uniaxial compression test in direction 1, respectively. Performing similar algebra for a test in direction 3

$$\begin{cases} \nu_{31}^{t} = \nu_{32}^{t} = \nu_{31}^{c} = \nu_{32}^{c} = \frac{1}{2} \\ Y_3^{t} = 2\left(\mu_{33}^{t} + \frac{1}{2}\mu_{11}^{c}\right) \\ Y_3^{c} = 2\left(\mu_{33}^{c} + \frac{1}{2}\mu_{11}^{t}\right) \end{cases} \tag{9}$$

where the subscripts indicate the respective axes and the superscripts t and c mean tension and compression, respectively. Considering tension and compression in the muscle fibre and cross fibre directions shows that only four of these constants are independent. From these equations we can determine μ_{11}^{c}, μ_{11}^{t}, μ_{33}^{c} and μ_{33}^{t}, to which μ_{13} is added. If we use the four Young's moduli to determine the material constants, the Poisson's ratios are automatically obtained as result. We now solve Eqs. $(7)_2$, $(8)_2$, $(9)_2$ and $(9)_3$ taking the reference Young's moduli in the underformed configuration from the experimental data from chicken pectoralis muscle, provided in Mohammadkhah et al. (2016), which we have measured approximately as

$$Y_1^{t} = 163 \text{ kPa}, \quad Y_1^{c} = 2.95 \text{ kPa}, \quad Y_3^{t} = 100 \text{ kPa}, \quad Y_3^{c} = 2.70 \text{ kPa} \tag{10}$$

The tensile response is seen to be two orders of magnitude larger than in compression for both directions, as noted in Mohammadkhah et al. (2016). Moreover, chicken muscle tissue is most compliant in the fibre direction 3 (denoted *longitudinal* therein and labelled *L*) than in the cross-fibre direction 1 (denoted *transverse* therein and labelled *T*) for both tensile and compressive applied deformation. Using the experimental yield moduli, the previous equations give the solution[1]

$$\mu_{11}^{t} = 104 \text{ kPa}, \quad \mu_{11}^{c} = -40.4 \text{ kPa}, \quad \mu_{33}^{t} = 70.2 \text{ kPa}, \quad \mu_{33}^{c} = -50.6 \text{ kPa} \tag{11}$$

which in turn result in the following (not independent) Poisson's ratios

$$\nu_{13}^{t} = 0.44 \quad \text{and} \quad \nu_{13}^{c} = 0.60 \tag{12}$$

These transverse-to-axial strain ratios are different to those actually observed in the tissue (see Table 3 in Mohammadkhah et al., 2016, namely $\nu_{13}^{t} \equiv \nu_{TL}^{t} \approx 0.83$ and $\nu_{13}^{c} \equiv \nu_{TL}^{c} \approx 0.34$). These are given for larger deformation levels and in terms of logarithmic strain ratios, hence they are not directly comparable with the present solution. These differences in computed continuum Poisson's ratios and experimental ones could be explained in part from the fact that they have been predicted using a purely continuum theory, assuming a sufficiently large scale such that the continuum principles hold, whereas in muscle the size of the specimen may be relevant in the observed behavior at larger than usual scales (Meyer and Lieber, 2011; Meyer et al., 2011; Gras et al., 2013). Furthermore, passive muscle behavior under compression is somewhat dictated by specimen size at the tissue level (Simms et al., 2017) where, additionally, the difficulty in imposing common boundary conditions for every specimen size, along with differences in fluid exudation, could have some adverse effects. Since our model captures exactly the tests presented to the model, all the mentioned discrepancies are reflected in the Poisson ratios.

The deviatoric moduli given in Eq. (11) include two positive moduli associated with both tension branches in Eq. (2) and two negative moduli associated with both compression branches in Eq. (2). Traditional isochoric hyperelastic models, based on continuously differentiable analytical hyperelastic functions, are unable to include this type of positive-tension/negative-compression asymmetry. Importantly, the solution encountered herein in an infinitesimal scenario may explain why experimental data from this specific type of skeletal muscle has not

[1] Two more solutions are obtained, but they are rejected because yield negative Poisson ratios as a consequence, which is in contradiction with the initial hypotheses considered herein (see, for example, Eqs. (5) and (6)) based on experimental evidence (Mohammadkhah et al., 2016).

been captured by current constitutive modelling approaches using a single set of material parameters (Mohammadkhah et al., 2016). We emphasize that the current infinitesimal theory is not a model, but the general continuum theory for transversely isotropic incompressible materials at small strains, just incorporating the possibility of different moduli in tension and compression. We also remark that the combination of all of the *internal* deviatoric moduli $\mu_{ij}^{t/c}$ (which cannot be directly observed experimentally) yield the four *positive* Young's moduli given in Eq. (10), which are the actual experimental observations. Indeed, any other observable moduli can equally be derived from the internal moduli. For example, transverse shear is likely to occur at the tissue level when the muscle is deformed within the transversely isotropic plane. For a linear material, the shear modulus in the isotropic plane is, evidently, the deviatoric modulus $G_{12} = \mu_{11}$. For a bilinear material, this expression is readily generalized as $G_{12} = 1/2(\mu_{11}^{t} + \mu_{11}^{c})$. If we specialize this expression to the present chicken pectoralis data, we obtain $G_{12} = 1/2(104 - 40.4) = 31.8$ kPa, which is positive again.

Nonetheless, it may still be somewhat surprising that there are two negative *internal* moduli in Eq. (11). The equations presented are a continuum theory but they cannot directly provide explanations, which require the consideration of microstructural effects.

Muscle is composed of a fluid phase (mainly water) and a solid one, similar to soils. The fluid phase is incompressible. A tentative decrease of the occupied fluid volume increases the fluid pressure. The effect of the fluid pressure in soils is to decrease the load transmitted by the soil reducing the shear capacity of the soil. This effect, in a continuum setting, is accounted for by the effective stress concept (known as Terzaghi decomposition), which is the stress carried by the skeleton referred to the total volume, see Fig. 1a.

Consider a tension test in a solid with an internal fluid as shown in Fig. 1b. Assume that the fluid pressure increase β is a linear function of the uniaxial strain ε, i.e. $\beta = F\varepsilon > 0$, with the constant F relating the pressure build-up in the internal fluid with the longitudinal stretch in the muscle during the tensile test. The equilibrium equation in the reference total domain is

$$\sigma = \sigma_s - \beta \tag{13}$$

where σ is the continuum stress exerted by the grips and σ_s is the load carried by the solid phase. The apparent modulus is

$$\frac{d\sigma}{d\varepsilon} = \frac{d\sigma_s}{d\varepsilon} - \frac{d\beta}{d\varepsilon} \;\Rightarrow\; Y = Y_s - F \tag{14}$$

where Y_s is the Young modulus of the solid phase, $F = d\beta/d\varepsilon$ and Y is the apparent (continuum) modulus. From this equation it is clear that if $F > 0$ then $Y < Y_s$, and it may even happen that $Y < 0$ with $Y_s > 0$. Hence a negative continuum (apparent) modulus does not imply that the solid phase has a negative value. Furthermore, we note that from Y alone, it is not possible to uniquely determine Y_s and F, but only their combined effect. A reason for the potential volume decrease in muscle is given in Gindre et al. (2013). Muscle consists of fibres surrounded by connective tissues. Collagen fibers in the connective tissue have a distribution of helices wrapped around muscle. As shown in Gindre et al. (2013) and Sleboda and Roberts (2017), due to the high stiffness of the collagen fibers and the helicoidal distribution, an increase in length results in an 'attempted' decrease of the fluid volume (consider Fig. 3 of Gindre et al., 2013) and an increase in the fluid pressure. That pressure β depends on the transverse properties of the solid phase and on the longitudinal strain exerted in the specimen, i.e. $\beta = F\varepsilon$.

In the 3D case given by Eqs. (4)–(6), we can perform the biphasic decomposition inserting the fluid pressure and follow again the same steps to arrive at equations of the type

$$Y_{33}^{t} = \frac{\sigma_3}{\varepsilon_3} = 2\left[\mu_{33\,s}^{t} + \frac{1}{2}\left(\mu_{11\,s}^{c} - \frac{\beta}{\varepsilon_3}\right)\right] \tag{15}$$

where $\beta/\varepsilon_3 = F$ and $\mu_{iis}^{t/c}$ correspond to moduli in the solid phase. This Equation is to be compared to continuum Eq. (9) which was obtained without the biphasic decomposition. We can interpret

$$\mu_{11}^{c} = \mu_{11\,s}^{c} - F \tag{16}$$

which may result in $\mu_{11} < 0$ if $F > \mu_{11\,s}^{c}$, even when $Y_{33}^{t} > 0$. As in the uniaxial case, we cannot determine $\mu_{iis}^{t/c}$ from the continuum measures, but only the combined effects given by the apparent constants.

A qualitatively similar explanation for negative internal moduli is given in Buckley et al. (2013) for the observed influence of fluid pressure in tendon. However, the influence of the fluid pressure of the tissue in the stress recorded during a tensile test is not well understood, and has been related to the micromechanics of the tissue, see for example (Buckley et al., 2013; Willems et al., 1999; Masic et al., 2015; Wess and Orgel, 2000) and therein references. In tendon, osmotic pressure induces tensile forces in tendon collagen which surpass by orders of magnitude that generated by contractile muscles (Masic et al., 2015).

2.3. Tension/compression uniaxial test at 45°

The procedure to determine the remaining material constant μ_{13} from a uniaxial test performed at 45° with respect to the fibre direction 3 is just a particularization to the small strain linear case of the more general procedure detailed in Romero et al., (2017). We can determine this material constant from either the tension test, as done in Romero et al., (2017) or the compression test. Similar conclusions are obtained, but both branches cannot be simultaneously captured with the transversely isotropic model. Note that $\omega_{13} < (E_{13}^{\#})$ must be symmetric by invariance principles. Once the shear moduli μ_{13} has been obtained from one of these branches, then the other experimental branch is predicted by the model.

The particularization of the generally nonlinear governing equations of Romero et al., (2017) to the present bi-linear case is achieved substituting logarithmic strains with infinitesimal strains and using $\alpha \equiv 45°$

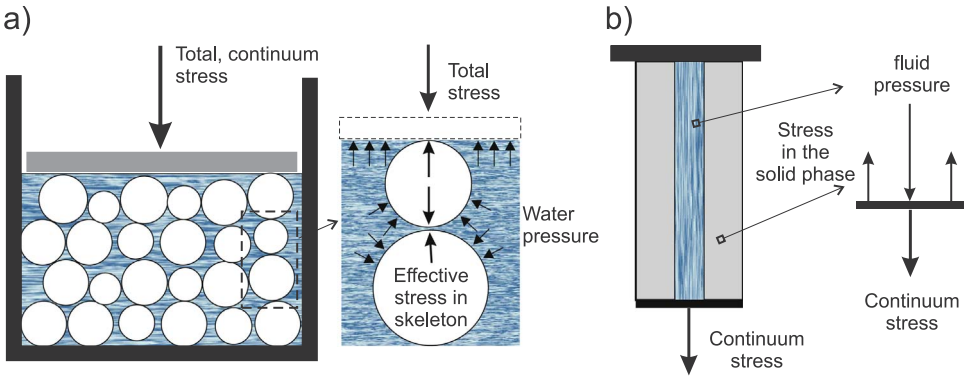

Fig. 1. (a) The concept of effective stress in the soil skeleton. (b) Stress in the solid phase upon an increase of fluid pressure.

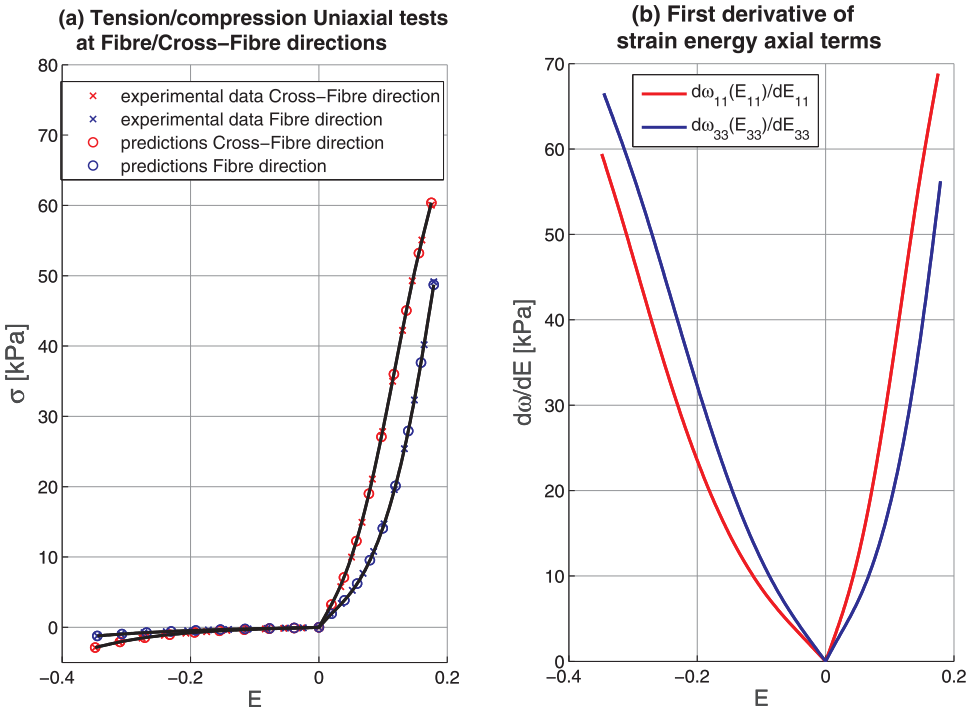

Fig. 2. (a) Experimental data (from Ref. Mohammadkhah et al., 2016) and model exact predictions for the tension/compression uniaxial tests along fibre and cross-fibre directions of chicken pectoralis muscle. (b) First derivative spline-based functions of the solution strain energy axial terms of Eq. (24). The slope of the curves in Fig (b) are, for each strain value, the corresponding instantaneous internal modulus; for example $\omega''_{11}(E_{11}=0^+)=2\mu^t_{11}$. Note that the energy terms are piece-wise splines, so a compact closed form is not possible. The plots in (b) give the piece-wise splines (cubic polynomials), in graphical form. These splines can be employed to compute the response in any other loading situation.

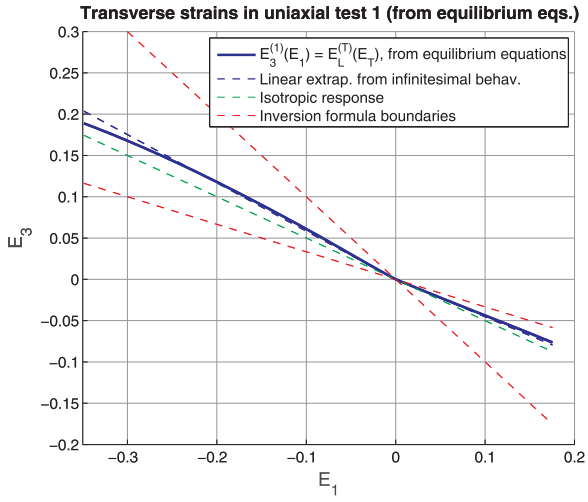

Fig. 3. Transverse-to-axial strains $E_3(E_1)\equiv E_L(E_T)$ obtained as a part of the strain energy determination procedure. Axis 3 corresponds to the fibre direction and axis 1 corresponds to the cross-fibre direction. The slope, at each strain value, is (minus) the equivalent instantaneous Poisson's ratio defined in terms of logarithmic strains, which is obtained by compatibility from the computed solution.

$$\sigma^t_\alpha(\varepsilon_1)=(\mu^t_{11}+\mu^t_{33}+4\mu^c_{11})\varepsilon_1+(\mu^t_{11}+\mu^t_{33}+4\mu^c_{11})\varepsilon_3 \tag{17}$$

and

$$\sigma^t_\alpha(\varepsilon_1)=2\omega'_{13}\left(\frac{\varepsilon_1-\varepsilon_3}{2}\right)=2\mu_{13}(\varepsilon_1-\varepsilon_3) \tag{18}$$

where, very importantly in this case for the proper consideration of the corresponding tension/compression branch to be used, we assume a transverse contraction $\varepsilon_2=-\varepsilon_1-\varepsilon_3<0$. In these equations, the measured strains ε_1 and stresses σ^t_α during the tensile test relate through $\sigma^t_\alpha(\varepsilon_1)=Y^t_\alpha\varepsilon_1$, where Y^t_α is the uniaxial tensile modulus. Then, from Eq. (17), and a similar one in compression, we obtain the in-plane transverse strain ε_3 for each input value $\varepsilon_1>0$ or $\varepsilon_1<0$ as

$$\varepsilon_3=-\nu^{\alpha t}_{13}\varepsilon_1 \quad \text{or} \quad \varepsilon_3=-\nu^{\alpha c}_{13}\varepsilon_1 \tag{19}$$

with

$$\nu^{\alpha t}_{13}=\frac{\mu^t_{11}+\mu^t_{33}+4\mu^c_{11}-Y^t_\alpha}{\mu^t_{11}+\mu^t_{33}+4\mu^c_{11}} \quad \text{or} \quad \nu^{\alpha c}_{13}=\frac{\mu^c_{11}+\mu^c_{33}+4\mu^t_{11}-Y^c_\alpha}{\mu^c_{11}+\mu^c_{33}+4\mu^t_{11}} \tag{20}$$

being the *observed* Poisson's ratios of the uniaxial tension/compression tests performed at $\alpha=45°$. Note that we need the material constants $\mu^{t/c}_{11}$ and $\mu^{t/c}_{33}$, computed as described in the previous subsection, and that the solution obtained is valid provided that $\nu^{\alpha\ t/c}_{13}<1$. Finally, Eq. (18) and a similar one for compression give

$$Y^t_\alpha=2\mu_{13}(1+\nu^{\alpha t}_{13}) \quad \text{and} \quad Y^c_\alpha=2\mu_{13}(1+\nu^{\alpha c}_{13}) \tag{21}$$

both of which may be used to determine μ_{13}. Note that these expressions mimic the relation $Y=2\mu(1+\nu)$ among the Young modulus Y, the Poisson's ratio ν and the shear modulus μ in classical isotropic elasticity.

We specialize now Eqs. (21) and (20) to the experimental data from chicken pectoralis muscle, provided in Mohammadkhah et al. (2016). The consideration of the uniaxial compression test modulus ($Y^c_\alpha=2.58$ kPa) yields

$$\nu^{\alpha c}_{13}=0.99 \tag{22}$$

and

$$\mu_{13}=\frac{Y^c_\alpha}{2(1+\nu^{\alpha c}_{13})}=0.648 \text{ kPa} \tag{23}$$

which are rather realistic values at small strains.

3. Transversely isotropic finite strain response

We now extend the analysis to the finite strain framework using a purely phenomenological WYPiWYG transversely isotropic hyperelasticity model (Latorre and Montáns, 2013, 2014; Crespo et al., 2017) based on logarithmic strains. This captures in an *exact* manner four uniaxial tension/compression asymmetric stress-strain nonlinear branches in material preferred directions and one uniaxial stress-strain nonlinear branch along the fibre orientation at 45°. The same conceptual results discussed above are obtained in this case, which manifests the importance of recovering the infinitesimal framework to be

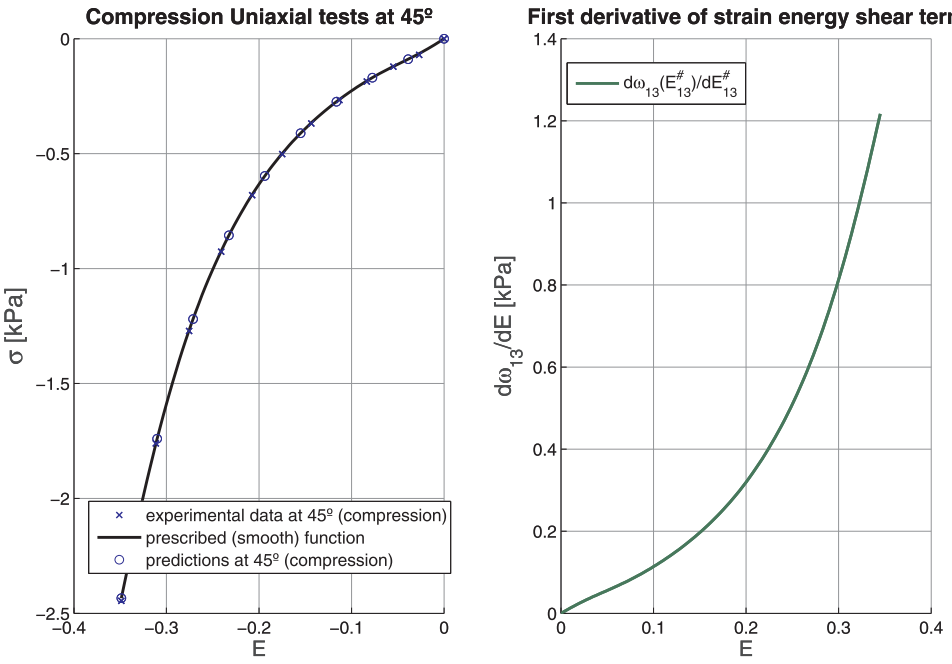

Fig. 4. (a) Experimental data (from Ref. Mohammadkhah et al., 2016) and model exact predictions for the compression uniaxial test performed along the fibre orientation of 45°. (b) First derivative spline-based function of the solution strain energy shear term of Eq. (24). This solution has been obtained using experimental data from the compression branch of the uniaxial test of Fig. 4a.

able to use engineering procedures to understand the ongoing phenomena.

Consider an incompressible transversely isotropic material with different axial behavior in tension and compression along its preferred material directions, as the one shown in Mohammadkhah et al. (2016) for chicken pectoralis muscle. We can characterize this material from a phenomenological perspective employing a single isochoric strain energy function of the logarithmic isochoric strain tensor $\mathbf{E} = \frac{1}{2}\ln(\mathbf{C})$, where $\mathbf{C}$ is the isochoric right Cauchy-Green deformation tensor, of the form

$$\mathscr{W}(E_{11}, E_{22}, E_{33}, E^{\#}_{13}) = \omega_{11}(E_{11}) + \omega_{11}(E_{22}) + \omega_{33}(E_{33}) + 2\omega_{13}(E^{\#}_{13}) \tag{24}$$

with $\omega_{ii}(E)$, $i = \{1, 3\}$, being generally non-symmetric, non-linear functions capable of including any kind of tension/compression asymmetry effects and $\omega_{13}(E^{\#}_{13})$ being a single-branch non-linear function capable of capturing the symmetric shear behavior in preferred planes. The five non-linear strain energy branches included in Eq. (24) characterize the generally non-linear strain-stress material response. We emphasize that the uncoupled form of Eq. ((24) is not a constraint of the WYPiWYG procedure, but the one compatible with the infinitesimal theory at all strain levels that may be determined with the available tests. Including additional strain component couplings in the stored energy would require additional tests.

We consider both tension and compression uniaxial tests along both cross-fibre and fibre directions, i.e. four uniaxial tests from which we should be able to determine the two tension/compression non-linear functions $\omega_{ii}(E)$. We solve the non-linear system of governing equations for these uniaxial tests, reported in Latorre and Montáns (2013), taking the chicken pectoralis muscle experimental data provided in Mohammadkhah et al. (2016). The prescribed experimental data is given in Fig. 2a in terms of principal logarithmic strains and Cauchy stresses. We solve the governing equations in an exact way following the enhanced algorithm provided in Romero et al..

The first derivative functions $\omega'_{ii}(E)$ obtained as the *unique* solution satisfying the corresponding equilibrium equations with transverse contraction are shown in Fig. 2b. In this case the transverse-to-axial strain relations are obtained as a part of the solution of the non-linear system of equations. Both tension/compression branches of the transverse-to-axial strain relation $E_3(E_1) = E_L(E_T)$, which generalizes the Poisson's ratio ν_{TL} effects in the foregoing small strain analysis, are shown in Fig. 3. The small strain limits ${\nu_{TL}}^c$ and ${\nu_{TL}}^t$ are consistently obtained. The relation $E_3(E_1)$, obtained as a byproduct of the computational procedure, results to be slightly non-linear in terms of logarithmic strains.

The uniaxial stresses that the strain energy terms of Fig. 2b, along with the transverse strains of Fig. 3, predict for the chicken pectoralis skeletal muscle under study are also shown in Fig. 2a. To the best of the authors' knowledge, this is the first hyperelastic formulation that is able to exactly capture such a significant tension/compression asymmetry effect within the whole deformation domain along preferred material directions.

Recall now the solution for deviatoric moduli given in Eq. (11). Equivalently, we observe in Fig. 2b that the branches of both functions $\omega'_{ii}(E)$ present positive slope (i.e. positive deviatoric local moduli) for the whole tension domain $E > 0$ and negative slope (i.e. negative deviatoric local moduli) for the whole compression domain $E < 0$. However, the corresponding combination of these strain energy branches during the uniaxial tests yield the four *positive* stiffness branches $d\sigma_{ii}/dE_{ii}$ shown in Fig. 2a (i.e. positive local Young's moduli).

We now determine the remaining non-linear term $\omega'_{13}(E)$ from a uniaxial test performed at an orientation of $\alpha = 45°$ with respect to the fibre direction 3. We follow the procedure detailed in Ref. Romero et al., (2017) but using the uniaxial compression stress–strain data provided in Mohammadkhah et al. (2016).

We show in Fig. 4a the prescribed stress–strain data points. In Fig. 4b we show the solution non-linear shear term $\omega'_{13}(E)$ present in Eq. (24), which again solves the governing equations of this test in an exact way, see predictions for $\sigma^c_\alpha(E)$ in Fig. 4a.

Therefore, the present transversely isotropic formulation exactly captures the five independent branches that are needed to characterize a tension/compression asymmetric incompressible transversely isotropic material, see Figs. 2a and 4a. This result is parallel to that encountered within the respective small strain characterization of the problem at hand.

However, we must mention that the overall Poisson ratios are not accurately captured, compare Fig. 3 with Mohammadkhah et al. (2016). There may be several reasons for this discrepancy. First, the different curves have been obtained averaging different specimens

because it is not possible to perform all the tests in the same specimen, so they do not correspond to a unique material. This may result in relevant inaccuracies (Robertson and Cook, 2014), Cook and Robertson (2016). Second, to avoid buckling, compression specimens have relatively large transverse dimensions, so the uniaxial boundary conditions may not be accurate. Third, and probably most importantly, the transverse isotropy assumption is only a modelling approximation of a possibly more anisotropic behavior due to the complexity of the extracellular matrix.

4. Conclusions

In-vitro experiments of the passive anisotropic behavior of chicken pectoralis muscle present a strong asymmetry which, to the best of authors' knowledge, has not previously been successfully captured by a model in the literature. In this work we have proposed a model capable of capturing that asymmetry and reproducing exactly up to five experimental tests using a single stored energy, despite some poor predictions of the Poisson's ratios. The somewhat surprising results, in which negative internal moduli are obtained, are confirmed by the applicable infinitesimal theory. However, much research is still to be done in order to fully understand the observed phenomena, which may be due to internal fluid pressure build-up during the tests and the complexity of the interaction between the muscle fibres and the extracellular matrix.

Acknowledgments

Partial financial support for this work has been given by grant DPI2015-69801-R from the Dirección General de Proyectos de Investigación of the Ministerio de Economía y Competitividad of Spain. FJM also acknowledges the support of the Department of Mechanical and Aerospace Engineering of University of Florida during the sabbatical period in which this paper was completed and Ministerio de Educación, Cultura y Deporte of Spain for the financial support for that stay under grant PRX15/00065.

Appendix A. Supplementary data

Supplementary data associated with this article can be found in the online version at http://dx.doi.org/10.1016/j.jmbbm.2017.09.012.

References

Buckley, M.R., Sarver, J.J., Freedman, B.R., Soslowsky, L.J., 2013. The dynamics of collagen uncrimping and lateral contraction in tendon and the effect of ionic concentration. J. Biomech. 46 (13), 2242–2249.

Cook, D.D., Robertson, D.J., 2016. The generic modeling fallacy: average biomechanical models often produce non-average results!. J. Biomech. 49 (15), 3609–3615.

Crespo, J., Latorre, M., Montáns, F.J., 2017. WYPIWYG hyperelasticity for isotropic, compressible materials. Comput. Mech. 59, 73–92.

Du, Z., Guo, X., 2014. Variational principles and the related bounding theorems for bimodulus materials. J. Mech. Phys. Solids 73, 183–211.

Du, Z., Zhang, Y., Zhang, W., Guo, X./, 2016. A new computational framework for materials with different mechanical responses in tension and compression and its applications. Int. J. Solids Struct. 100, 54–73.

Gindre, J., Takaza, M., Moerman, K.M., Simms, C.K., 2013. A structural model of passive skeletal muscle shows two reinforcement processes in resisting deformation. J. Mech. Behav. Biomed. Mater. 22, 84–94.

Gras, L.L., Mitton, D., Viot, P., Laporte, S., 2013. Viscoelastic properties of the human sternocleidomastoideus muscle of aged women in relaxation. J. Mech. Behav. Biomed. Mater. 27, 77–83.

Latorre, M., Montáns, F.J., 2013. Extension of the Sussman-Bathe spline-based hyperelastic model to incompressible transversely isotropic materials. Comput. Struct. 122, 13–26.

Latorre, M., Montáns, F.J., 2014. What-You-Prescribe-Is-What-You-Get orthotropic hyperelasticity. Comput. Mech. 53 (6), 1279–1298.

Van Loocke, M., Lyons, C.G., Simms, C.K., 2006. A validated model of passive muscle in compression. J. Biomech. 39 (16), 2999–3009.

Masic, A., Bertinetti, L., Schuetz, R., Chang, S.W., Metzger, T.H., Buehler, M.J., Fratzl, P., 2015. Osmotic pressure induced tensile forces in tendon collagen. Nat. Commun. 6, 5942.

Meyer, G.A., Lieber, R.L., 2011. Elucidation of extracellular matrix mechanics from muscle fibers and fiber bundles. J. Biomech. 44 (4), 771–773.

Meyer, G.A., McCulloch, A.D., Lieber, R.L., 2011. A nonlinear model of passive muscle viscosity. J. Biomech. Eng. 133 (9), 091007.

Moerman, K.M., Simms, C.K., Nagel, T., 2016. Control of tension-compression asymmetry in Ogden hyperelasticity with application to soft tissue modelling. J. Mech. Behav. Biomed. Mater. 56, 218–228.

Mohammadkhah, M., Murphy, P., Simms, C.K., 2016. The in vitro passive elastic response of chicken pectoralis muscle to applied tensile and compressive deformation. J. Mech. Behav. Biomed. Mater. 62, 468–480.

Robertson, D., Cook, D., 2014. Unrealistic statistics: how average constitutive coefficients can produce non-physical results. J. Mech. Behav. Biomed. Mater. 40, 234–239.

Romero, X., Latorre, M., Montáns, F.J., 2017. Determination of the WYPiWYG strain energy density of skin through finite element analysis of the experiments on circular specimens. Finite Elem. Anal. Des. 134, 1–15.

Simms, C., Kilroy, H., Blackburn, G., Takaza, M., 2017. The influence of physical dimension on apparent stress-strain behaviour of in vitro passive skeletal muscle samples. J. Strain Anal. Eng. Des. 52 (1), 3–11.

Sleboda, D.A., Roberts, T.J., 2017. Incompressible fluid plays a mechanical role in the development of passive muscle tension. Biol. Lett. 13 (1), 20160630.

Sussman, T., Bathe, K.J., 2009. A model of incompressible isotropic hyperelastic material behavior using spline interpolations of tension-compression test data. Commun. Numer. Methods Eng. 25 (1), 53–63.

Takaza, M., Moerman, K.M., Gindre, J., Lyons, G., Simms, C.K., 2013. The anisotropic mechanical behaviour of passive skeletal muscle tissue subjected to large tensile strain. J. Mech. Behav. Biomed. Mater. 17, 209–220.

Wess, T.J., Orgel, J.P., 2000. Changes in collagen structure drying, dehydrothermal treatment and relation to long term deterioration. Thermochim. Acta 365 (1), 119–128.

Willems, M.E., Huijing, P.A., Friden, J., 1999. Swelling of sarcoplasmic reticulum in the periphery of muscle fibres after isometric contractions in rat semimembranosus lateralis muscle. Acta Physiol. Scand. 165 (4), 347–356.

Zhang, L., Zhang, H., Wu, J., Yan, B., Lu, M., 2016. Parametric variational principle for bimodulus materials and its application to nacreous bio-composites. Int. J. Appl. Mech. 8 (06), 1650082.